Imbibition by polygonal spreading on microdecorated surfaces

LAURENT COURBIN[1], ETIENNE DENIEUL[1], EMILIE DRESSAIRE[1], MARCUS ROPER[1], ARMAND AJDARI[1,2] AND HOWARD A. STONE[1]*

[1]School of Engineering and Applied Sciences, Harvard University, Cambridge, Massachusetts 02138, USA
[2]Gulliver, UMR 7083, CNRS-ESPCI, 10 rue Vauquelin, 75005 Paris, France
*e-mail: has@seas.harvard.edu

Published online: 12 August 2007; doi:10.1038/nmat1978

Micropatterned surfaces have been studied extensively as model systems to understand influences of topographic[1] or chemical[2,3] heterogeneities on wetting phenomena. Such surfaces yield specific wetting or hydrodynamic effects, for example, ultrahydrophobic surfaces[4], 'fakir' droplets[5], tunable electrowetting[6], slip in the presence of surface heterogeneities[7,8] and so on. In addition, chemical patterns allow control of the locus, size and shape of droplets by pinning the contact lines at predetermined locations[9,10]. Applications include the design of 'self-cleaning' surfaces[11] and hydrophilic spots to automate the deposition of probes on DNA chips[12]. Here, we discuss wetting on topographically patterned but chemically homogeneous surfaces and demonstrate mechanisms of shape selection during imbibition of the texture. We obtain different deterministic final shapes of the spreading droplets, including octagons, squares, hexagons and circles. The shape selection depends on the topographic features and the liquid through its equilibrium contact angle. Considerations of the dynamics provide a 'shape' diagram that summarizes our observations and suggest rules for a designer's tool box.

Although most studies of wetting on patterned surfaces have concerned poorly wetting liquids for which the topography acts to generate 'super-hydrophobicity', as on a lotus leaf[11], we focus on hydrophilic surfaces where the excess solid surface from the roughness enhances the wettability thermodynamically[13] and in some cases kinetically[14]. For a droplet deposited on a microtextured surface, thermodynamic arguments yield three distinct types of behaviour depending on the equilibrium contact angle, $\theta_{eq} < \pi/2$, of the liquid on a flat surface of homogeneous surface chemistry[15,16]: (1) for $\theta_c < \theta_{eq}$, where the threshold θ_c depends on the characteristics of the roughness, hydrophilicity is enhanced and the macroscopic droplet lies on the microtextured surface with an effective contact angle lower than θ_{eq}; (2) for $0 < \theta_{eq} < \theta_c < \pi/2$, the liquid invades the surface by partial imbibition by the roughness, whereas the macroscopic droplet does not spread but progressively shrinks owing to the corresponding loss into the microtexture; and (3) only when $\theta_{eq} = 0$ is complete wetting achieved and the droplet spreads macroscopically. Here, we thoroughly study regime 2, and show that on regularly patterned surfaces (square arrays of circular posts with heights H, radii R and inter-post spacings, ℓ, of approximately 50 μm; Fig. 1a) the droplets exhibit ordered centimetre-size shapes, from circles to polygons (see the Methods section). We first extend some of the above-mentioned studies[15,16]: spreading by imbibition of the roughness with a non-spreading reservoir (Fig. 1b and Supplementary Information, Movie S1). We then demonstrate that the dynamics make this partial wetting regime very rich, with the selection of a variety of shapes of the wetted area depending on the geometrical features of the texture and the wetting properties of the liquid. As an example, Fig. 1c shows the transient spreading of a droplet, from an initial circle, through an octagon, to an equilibrium square shape. In what follows, we describe the basic elements necessary to understand and control such polygonal patterns.

We begin by varying the liquid and thus θ_{eq}. Drops of the same size, which are released on the same micropatterned surfaces, end up with different reproducible wetted areas and shapes. We find seven macroscopic scenarios (Fig. 2) as wettability (in this case, $\cos\theta_{eq}$) increases. In the first three (i–iii), the contact line gets pinned in a well-defined metastable shape, either (i) a circle, (ii) octagon or (iii) square, whereas the reservoir, whose shape is a spherical cap, remains of finite size. In the four others (iv–vii), imbibition empties the reservoir leaving a stable wetted domain, either (iv) a square, (v) octagon, (vi) rounded octagon or (vii) circle. Given the fact that we obtain identical polygonal shapes when pure liquids or mixtures of these liquids spread on rough surfaces having different ratio H/ℓ, the local composition of the liquid mixtures (for example, potentially producing variations in surface tension) does not play a role in our observations. These observations of anisotropic imbibition, including faceting (Fig. 1c), occur even though, at the macroscopic level, both the spreading coefficient[13] and the (low Reynolds number) hydrodynamic permeability of the square lattice are isotropic and homogeneous.

To explain the diversity of final wetted shapes, it is necessary to understand the dynamics of the contact line at the microscale of the individual posts. We follow the motion of the facets, which advance along the axes of the square pattern or along the diagonals, by using bright-field microscopy coupled with high-speed imaging (Fig. 3a and Supplementary Information, Movie S2). A slow motion (~150 ms) of the slightly curved contact line between two successive rows of posts ends when its front zone, which is often at the centre of the facet, reaches a dry post. Then this post is rapidly wet (~3 ms), followed by a lateral propagation of the corresponding 'steps' on the two sides, which fills out an 'edge', while continually there is slow motion of the wetting front. The large difference in timescales indicates that the spreading rate

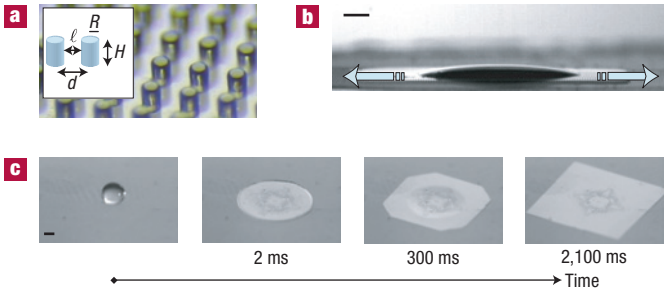

Figure 1 Mostly-wetting liquid droplets spreading over chemically homogeneous microtextured substrates form polygonal shapes. a, Schematic diagram of a micropatterned surface and photograph showing the surface topography. The diagram shows the radius, R, and height, H, of a cylindrical post, the lattice distance, d, and the inter-post spacings, ℓ. **b**, Side view of the spreading by imbibition of an isopropanol droplet on a microdecorated surface. The blue arrows indicate that the spreading proceeds in the texture with a non-spreading macroscopic reservoir. The lattice parameters are $d = 100\,\mu$m, $R = 25\,\mu$m and $H = 30\,\mu$m. **c**, A millimetre radius fluid droplet is released above the surface. The drop rapidly adopts an initial circular shape (~2 ms). The classical Washburn analysis of imbibition of porous media at the scale of a macroscopic drop, which is much larger than the scales of the pattern, predicts a subsequent isotropic invasion of the roughness[18]. Although at the macroscopic level the hydrodynamic permeability is isotropic and homogeneous we observe a transient octagon (~300 ms) and a final square shape (~2,100 ms). These pictures were taken obliquely at an angle of approximately 45°. The liquid is ethanol and the geometric parameters of the square lattice are $d = 100\,\mu$m, $R = 25\,\mu$m and $H = 60\,\mu$m. Scale bars: 1 mm.

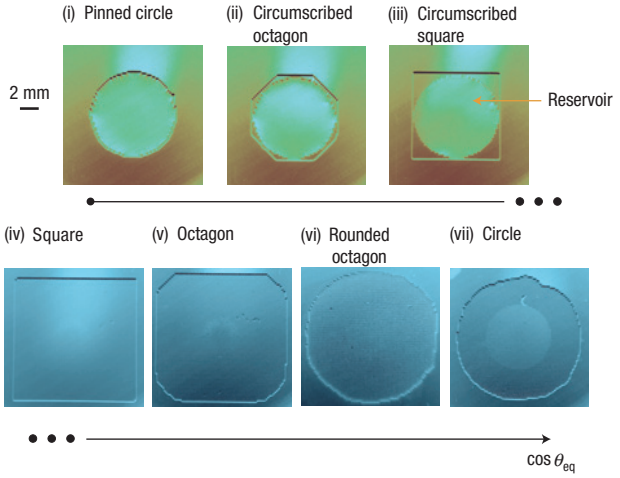

Figure 2 Final shapes for droplets of different liquids released on the same surface. A sequence of seven shapes for different liquid mixtures ordered by wetting properties and observed on one given patterned surface whose parameters are $d = 200\,\mu$m, $R = 50\,\mu$m and $H = 50\,\mu$m. The liquids are respectively: (i) ethanol ($\theta_{eq} \sim 35°$), (ii) 98 vol% ethanol and 2 vol% isopropanol ($\theta_{eq} \sim 32°$), (iii) 75 vol% ethanol and 25 vol% isopropanol ($\theta_{eq} \sim 30°$), (iv) 25 vol% ethanol and 75 vol% isopropanol ($\theta_{eq} \sim 27°$), (v) isopropanol ($\theta_{eq} \sim 25°$), (vi) hexane ($\theta_{eq} \sim 18°$), and (vii) silicone oil ($\theta_{eq} \sim 0°$). The threshold θ_c calculated by Bico *et al.*[15] using energy arguments is defined by $\cos\theta_c = (1-\phi_S)/(r-\phi_S)$, where $\phi_S = \pi R^2/d^2$ is the solid fraction on which a droplet rests and $r = 1 + 2\pi RH/d^2$ is the ratio of the real surface area to the horizontal projection of the surface area. This relation provides the value of the angle θ_c for the microdecorated surface in this figure, $\phi_S = 0.2$ and $r = 1.4$, which yields $\theta_c = 48°$. The estimate of θ_c is compatible with our experimental observations as even for the shape (i) the contact angle θ_{eq} is lower than θ_c. In addition, for this surface $H/\ell = 0.5$ gives a prediction for the contact angle $\theta_{eq} = \arctan(H/\ell) \sim 27°$ below which the contact line gets unpinned, which is in good agreement with our observations (the transition (iii) to (iv) occurs for $\theta_{eq} \sim 27$–$30°$). We have also carried out some experiments varying characteristics of the topography. For a given liquid (that is, $\cos\theta_{eq}$), the same shape is observed when both H and ℓ are changed in the same proportions to keep their ratio constant. Finally, a similar sequence of imbibition scenarios is obtained for a given liquid when the aspect ratio H/ℓ of the posts is increased; increasing the aspect ratio affects the shape in the same way as increasing $\cos\theta_{eq}$.

is controlled by the motion of the contact line over the scale ℓ. This stepwise propagation is similar to the 'pore invasion' mechanism for porous media in a Hele–Shaw geometry[17], although here we have a bottom solid surface and a free upper boundary.

As the dynamics are largely controlled by the speed at which the contact line reaches the next row of posts, we can rationalize the sequence of spreading scenarios (Fig. 2). The inter-post distance, ℓ, is shorter along the diagonal, $\ell_{di} = ((\sqrt{2}-1)/2)d$, than along the lattice axes, $\ell_{ax} = d/2$. Thus, we expect a slower motion along the latter direction. This geometrical difference suggests that pinning of the contact line occurs up to higher values of $\cos\theta_{eq}$ and/or higher aspect ratios H/ℓ along the axes than along the diagonal. Indeed, replacing the rows of posts by an infinite ridge (Fig. 3c), a pinned geometry corresponds to a flat interface contacting the bottom surface locally with the equilibrium angle θ_{eq} before it reaches the next post. Such a static two-dimensional situation corresponds to $H/\tan\theta_{eq} < \ell$. Computation of the exact thresholds requires a three-dimensional analysis, but will not alter the qualitative features.

We expect pinning to disappear as H/ℓ or $\cos\theta_{eq}$ increases, with a weaker threshold along the diagonal than along the axes. This prediction is consistent with observations in Fig. 2 on increase of wettability (that is, $\cos\theta_{eq}$): (i) first 'zipping' of the steps is prevented so that the initial circle is preserved, (ii) a few rearrangements ('zipping') can proceed but contact lines are pinned in both directions leaving an octagon circumscribed to the initial circle, (iii) increasing the wettability further allows unpinning along the diagonals, but not along the axes, so that the corresponding facets evolve and close the initial octagon into a square, and (iv) eventually both contact lines are unpinned and imbibition proceeds until the reservoir liquid is exhausted.

When the contact lines move, their velocity, V, is controlled by the progression over the bottom surface to the next row (Fig. 3a). In this case, V is given by a balance between capillary driving ($\gamma\cos\theta_{eq}/d$) and viscous resistance ($\eta LV/d^2$), where L is the distance to the reservoir (Fig. 3b); the estimate for the viscous resistance can be derived using Darcy's law for the liquid flowing through the porous texture. Hence, we obtain $V \sim (d\gamma/L\eta)\cos\theta_{eq}$. The prefactor in this relation is a non-dimensional function of the geometry that increases with both H/ℓ and $\cos\theta_{eq}$, necessarily goes to zero at the pinning threshold, and thus depends on the direction. With $V \cong \mathrm{d}L/\mathrm{d}t$ (neglecting slow shrinkage of the reservoir), the classical Washburn scaling[18] $V \propto t^{-1/2}$ is recovered, as documented on similar surfaces for capillary rise[15]. We validate our predictions in Fig. 3b for a growing octagon, namely $L \propto t^{1/2}$ in both directions, but with a larger prefactor along the diagonal.

Figure 3d shows the contact line velocities along the axes or diagonals, V_{ax} or V_{di}, normalized as $VL\eta/d\gamma$, against the parameter varied in the experiments, $\cos\theta_{eq}$ and/or H/ℓ. Whether a growing faceted shape remains an octagon or evolves into a square depends on the ratio of the contact line velocities, V_{di}/V_{ax}. If $V_{di}/V_{ax} > \sqrt{2}$, the diagonal facets shrink as they move too fast, whereas otherwise octagonal shapes are asymptotically stable.

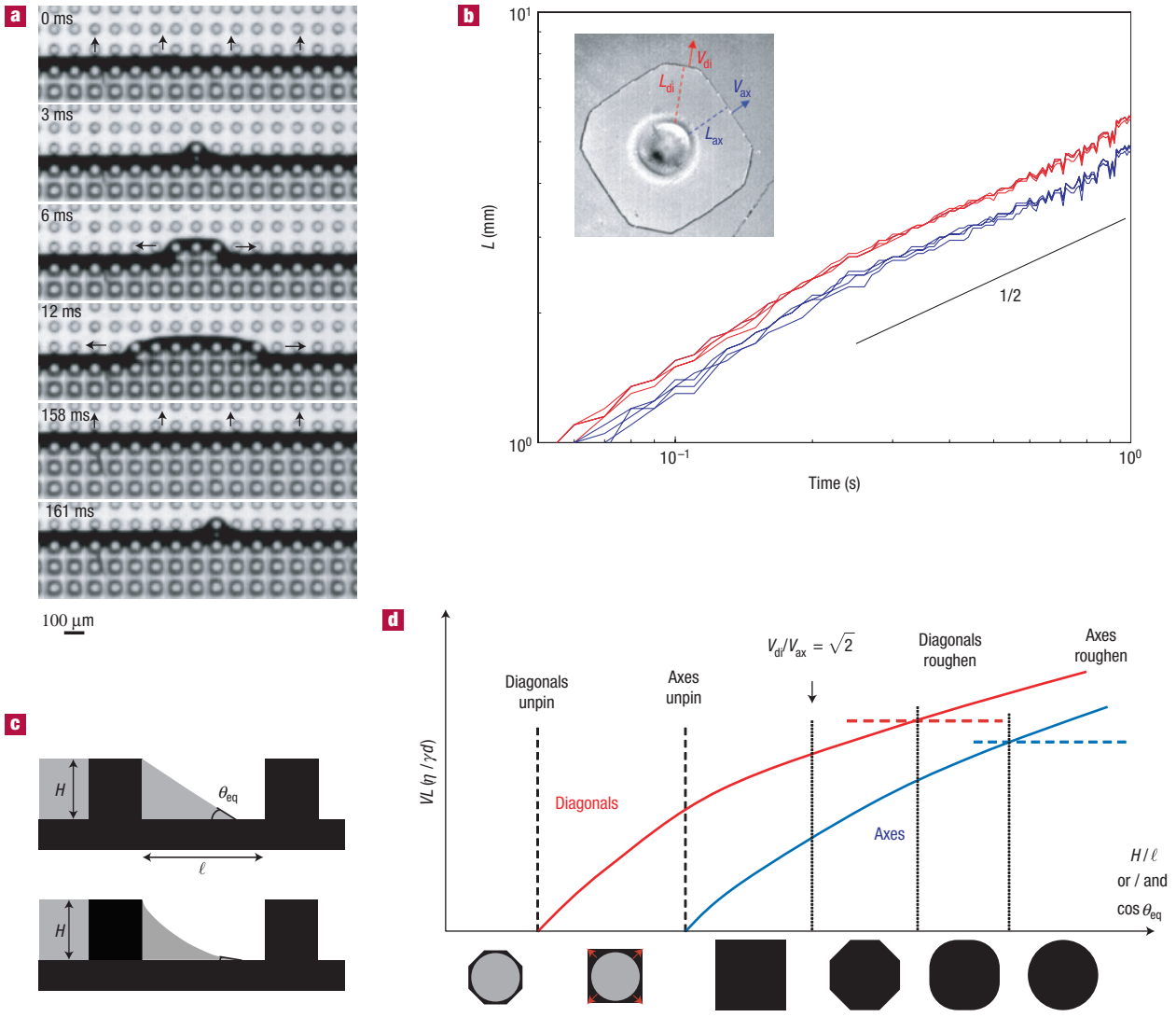

Figure 3 Dynamics of spreading provide a 'shape' diagram. a, Bright-field microscopic images of the motion of the contact line (isopropanol) at the scale of individual posts. The lattice parameters are $d = 100\,\mu m$, $R = 25\,\mu m$ and $H = 60\,\mu m$. **b**, Log–log plot of the distance, L, to the reservoir along the eight facets as a function of time. The colours correspond to different directions of the lattice: diagonals (red) and axes (blue). Inset: Top view of an isopropanol drop spreading on a microtextured surface defining the variables V_{di}, L_{di}, V_{ax} and L_{ax}. The lattice parameters are $d = 100\,\mu m$, $R = 25\,\mu m$ and $H = 60\,\mu m$. **c**, Schematic diagram of the contact line between two rows of posts. Top: Pinning in a configuration with zero mean curvature with equilibrium contact angle at the bottom. Bottom: Advancing contact line about to reach the next row. **d**, Schematic plot of the normalized contact line velocities along the diagonals (red curve) and the lattice axes (blue curve) as a function of $\cos\theta_{eq}$ and/or the post aspect ratio. The vertical dashed and dotted lines correspond to the transitions between each of the scenarios (ii) to (vii) described in Fig. 2.

This explains the transition from (iv) to (v) in Fig. 2: for effective wettabilities slightly larger than the unpinning threshold along the axes, V_{di}/V_{ax} is necessarily very large as the denominator is small, so the eventual shape is a square. For large wettabilities, the velocity ratio can become smaller than $\sqrt{2}$, yielding an octagon (in Fig. 3b, $V_{di}/V_{ax} \approx 1.3$). Accounting for the differences between L_{di} and L_{ax} at the square to octagon ((iv)–(v)) transition, a simple geometrical analysis locates this transition in Fig. 3d at the point where $V_{di}/V_{ax} = \sqrt{2}$.

The two last shape changes in Fig. 2 can be viewed as 'roughening transitions' for each type of facet. These dynamics correspond to the generation of new pairs of steps with rates $\sqrt{2}V_{di}/d$ and V_{ax}/d becoming comparable to the lateral propagation of the steps sideways over a few periods, leading to a finite density of steps and thus to curved interfaces. Although a more complete picture would require a comparison of the step propagation rates on the two facets, it is not unreasonable that this transition occurs first along the diagonal.

We conclude with some consequences of this analysis. In contrast to chemical patterning, the present method does not depend on the pinning of the contact line at a predetermined locus, but rather relies on the dynamics of spreading/imbibition to generate desired shapes. Consequently, topographical patterning offers possibilities not accessible with chemical patterning, namely (1) for a given liquid, the same shape is obtained wherever it is released (Fig. 4a), (2) different shapes can be obtained by changing the liquid (Fig. 4b) and (3) the drop volume controls the size of the wetted area (Fig. 4c). Changing the symmetry of

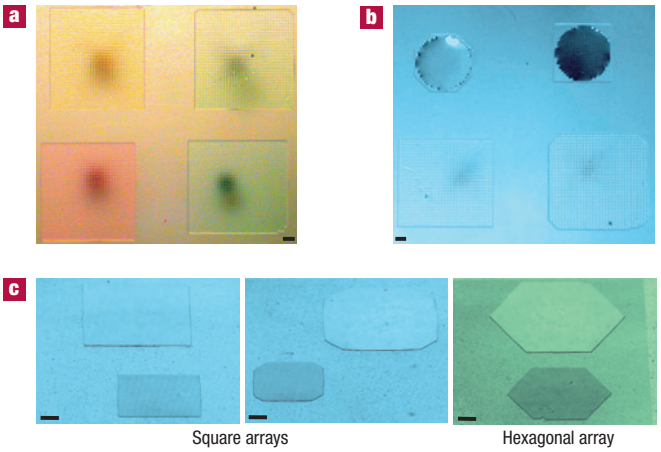

Figure 4 The design of the microtexture allows for the control of the locus, size and shape of spreading droplets. a, Four droplets of the same fluid coloured with different dyes give identical squares. **b**, Four different fluids spreading over a given microtextured surface exhibit different shapes (circumscribed square and octagon, square and octagon). The liquids are respectively: (circumscribed octagon) 98 vol% ethanol and 2 vol% isopropanol, (circumscribed square) 75 vol% ethanol and 25 vol% isopropanol, (square) 25 vol% ethanol and 75 vol% isopropanol, and (octagon) isopropanol. **c**, Two droplets of the same fluid on the same rough surface exhibit the same shapes (squares, octagons on a square lattice and hexagons on a hexagonal array) but with different sizes as the volume of the drop is changed. We used ethanol to form the squares and isopropanol for the octagons and hexagons. Scale bar: 1 mm. The parameters of the surface are $d = 200\,\mu$m, $R = 50\,\mu$m, $H = 50\,\mu$m for **a**,**b** and $d = 100\,\mu$m, $R = 25\,\mu$m, $H = 60\,\mu$m for **c**.

the topography can increase the tool box: other regular arrays can yield different shapes, for example, hexagons (Fig. 4c). Further modifications of the surface geometry should increase the number of realizable shapes.

METHODS

The microdecorated surfaces consist of square or hexagonal arrays of cylindrical posts made of polydimethylsiloxane transparent elastomers manufactured using soft-lithography techniques[19]. The lattice distance is $d = 100\,\mu$m or $d = 200\,\mu$m, the post radius $R = d/4$ and different post heights, H, which yields aspect ratios $H/\ell = 0.5, 0.6, 1.2$. We use mostly-wetting liquids for which the equilibrium contact angle, θ_{eq}, that the liquid makes with a smooth sample of polydimethylsiloxane is small but finite: $10° < \theta_{eq} < 35°$. These fluids include hexane (Sigma, purity 99+%), ethanol (Pharmaco-AAPER, purity 95+%) and isopropanol (VWR International, purity 99+%), and binary mixtures of these fluids for which we vary the respective volume fractions to tune the value of θ_{eq}. We use silicone oil (Sigma-Aldrich, polydimethylsiloxane 200 fluid) to achieve complete wetting ($\theta_{eq} = 0°$). A syringe filled with the liquid was mounted on a flow-rate-controlled syringe pump. A polyethylene tube was connected from the syringe to a needle at the end of which a liquid droplet was created and released from a specific height on the microtextured surface. The value of the height of release, 20 cm, is (1) small enough to prevent splashing during the impact and (2) large enough so that the impact dynamics produce an initial rapid macroscopic spreading of the drop over the surface, which leads to an almost circularly symmetric 'initial condition' and is essentially independent of the liquid used. We follow the time-dependent spreading with a high-speed camera (Phantom V9) working at a frame rate of 1,000−10,000 frame s^{-1}.

Received 19 February 2007; accepted 9 July 2007; published 12 August 2007.

References

1. Quéré, D. Non-sticking drops. *Rep. Prog. Phys.* **68**, 2495–2532 (2005).
2. Cubaud, T. & Fermigier, M. Faceted drops on heterogeneous surfaces. *Europhys. Lett.* **55**, 239–245 (2001).
3. Cubaud, T., Fermigier, M. & Jenffer, P. Spreading of large drops on patterned surfaces. *Oil Gas Sci. Technol. Rev. IFP* **56**, 23–31 (2001).
4. Onda, T., Shibuichi, N., Satoh, N. & Tsuji, K. Super-water-repellent fractal surfaces. *Langmuir* **12**, 2125–2127 (1996).
5. Quéré, D. Fakir droplets. *Nature Mater.* **1**, 14–15 (2002).
6. Krupenkin, T. N., Taylor, J. A., Schneider, T. M. & Yang, S. From rolling ball to complete wetting: The dynamic tuning of liquids on nanostructured surfaces. *Langmuir* **20**, 3824–3827 (2004).
7. Cottin-Bizonne, C., Barrat, J. L., Bocquet, L. & Charlaix, E. Low-friction flows of liquid at nanopatterned interfaces. *Nature Mater.* **2**, 237–240 (2003).
8. Lauga, E. & Stone, H. A. Effective slip in pressure-driven Stokes flow. *J. Fluid Mech.* **489**, 55–77 (2003).
9. Abbott, N. L., Folkers, J. P. & Whitesides, G. M. Manipulation of the wettability of surfaces on the 0.1 to 1-micrometer scale through micromachining and molecular self-assembly. *Science* **257**, 1380–1382 (1992).
10. Gau, H., Herminghaus, S., Lenz, P. & Lipowski, R. Liquid morphologies on structured surfaces: From microchannels to microchips. *Science* **283**, 46–49 (1999).
11. Barthlott, W. & Neinhuis, C. Purity of the sacred lotus, or escape from contamination in biological surfaces. *Planta* **202**, 1–8 (1997).
12. Blanchard, A. P., Kaiser, R. J. & Hood, L. E. High-density oligonucleotide arrays. *Biosens. Bioelectron.* **11**, 687–690 (1996).
13. de Gennes, P. G. Wetting: Statics and dynamics. *Rev. Mod. Phys.* **57**, 827–863 (1985).
14. McHale, G., Shirtcliffe, N. J., Aqil, S., Perry, C. C. & Newton, M. I. Topography driven spreading. *Phys. Rev. Lett.* **93**, 036102 (2004).
15. Bico, J., Tordeux, C. & Quéré, D. Rough wetting. *Europhys. Lett.* **55**, 214–220 (2001).
16. Bico, J. Mécanismes d'imprégnations: Surfaces texturées, bigouttes, poreux. Thesis, Univ. de Paris VI (2000).
17. Lenormand, R. Liquids in porous media. *J. Phys. Condens. Matter* **2**, SA79–SA88 (1990).
18. Washburn, E. W. The dynamics of capillary flow. *Phys. Rev.* **17**, 273–283 (1921).
19. McDonald, J. C. & Whitesides, G. M. Poly(dimethylsiloxane) as a material for fabricating microfluidic devices. *Acc. Chem. Res.* **35**, 491–499 (2002).

Acknowledgements

The authors thank D. Lohse, M. Fermigier, D. Quéré and M. Sbragaglia for helpful conversations. We thank the Harvard MRSEC (DMR-0213805) for support of this research.
Correspondence and requests for materials should be addressed to H.A.S.
Supplementary Information accompanies this paper on www.nature.com/naturematerials.

Competing financial interests

The authors declare no competing financial interests.